ISSN 0016-7029, Geochemistry International, 2011, Vol. 49, No. 5, pp. 429–438. © Pleiades Publishing, Ltd., 2011.
Original Russian Text © A.A. Kadik, N.A. Kurovskaya, Yu.A. Ignat'ev, N.N. Kononkova, V.V. Koltashev, V.G. Plotnichenko, 2011, published in Geokhimiya, 2011, Vol. 49, No. 5, pp. 451–461.

Influence of Oxygen Fugacity on the Solubility of Nitrogen, Carbon, and Hydrogen in $FeO–Na_2O–SiO_2–Al_2O_3$ Melts in Equilibrium with Metallic Iron at 1.5 GPa and 1400°C

A. A. Kadik[a], N. A. Kurovskaya[a], Yu. A. Ignat'ev[a], N. N. Kononkova[a], V. V. Koltashev[b], and V. G. Plotnichenko[b]

[a] *Vernadsky Institute of Geochemistry and Analytical Chemistry, Russian Academy of Sciences, ul. Kosygina 19, Moscow, 119991 Russia*
e-mail: kadik@geokhi.ru

[b] *Research Center of Fiber Optics, Russian Academy of Sciences, ul. Vavilova 38, Moscow, 11933 Russia*

Received November 3, 2010

Abstract—It is assumed in the theories of Earth formation that the composition of gases extracted by primary planetary magmas is formed by the large-scale melting of the early mantle, which occurred in the presence of a metallic Fe phase. The molten Fe metal and silicate materials underwent gravitational migration, which affected the fractionation of siderophile elements. Volatile compounds had to form simultaneously in the zones of large-scale melting of the early Earth; their compositions were controlled by interaction with silicate and metallic melts. This process remains poorly understood.

A series of experiments was carried out in the system silicate melt ($FeO–Na_2O–SiO_2–Al_2O_3$) + liquid metallic Fe + C (graphite) + volatile components (N–C–H) at 1.5 GPa, 1400°C, and oxygen fugacity (fO_2) 1.9 to 3.7 logarithmic units below the fO_2 value of the IW buffer equilibrium for the investigation of the simultaneous dissolution of N, C, and H in iron-bearing silicate melts. The mechanisms of N, C, and H dissolution were elucidated using the Raman spectroscopy of glasses produced by quenching of reduced melts. It was established that melting in the $T–F–fO_2$ stability range of the metallic phase results in the formation of species with N–H (NH_3), C–H (CH_4), and H–O (H_2O, OH^-) bonds and molecular N_2 and H_2 in silicate melts. Experimental investigations revealed a significant effect of pressure and fO_2 on the partitioning of N between silicate melt and equilibrium metallic phase ($D_N = N^{metal}/N^{silicate}$). At 1.5 GPa, 1400°C, and $\Delta \log fO_2$ (IW) values of −2.4 and −3.7, D_N is 2.9 and 0.5, respectively.

Keywords: experiment, solubility of volatiles, iron-bearing silicate melt, oxygen fugacity.
DOI: 10.1134/S001670291105003X

PROBLEM

Recent physical models of Earth formation postulate that the Earth experienced numerous collisions during accretion. Energy released in impact events is sufficient for the melting of considerable volumes of the silicate mantle and the formation of an outer molten layer (magma ocean) [1–3]. It is supposed that the magma ocean was related to the formation of the planetary core by the gravitational migration of metallic iron in the liquid silicate material of the mantle [4–7]. The segregation of iron in the zones of large-scale melting of the early Earth had to be accompanied by the formation of volatile compounds, the composition of which was controlled by the interaction of C, N, H, and O components with silicate and metallic melts. These reactions are still poorly known. Within the magma ocean concept, the formation of volatile components in the early Earth must depend on the character of dissolution of C, N, H, and O components in magmatic melts and molten Fe at oxygen fugacity (fO_2) values 5–8 orders of magnitude lower than those in the magmas of the present-day mantle [7–9].

It is suggested that the evolution of the early mantle and the magma ocean was accompanied by self-oxidation with an increase in fO_2 owing to Fe, Si, and O fractionation between silicate and metallic phases [10–14]. It was hypothesized [7, 11, 14] that the fO_2 increase in the magma ocean was due to FeO disproportionation during the crystallization of perovskite, $(Mg,Fe,Al)(Al,Si)O_3$, according to the reaction

$$3Fe^{2+}O(\text{melt}) + Al_2O_3(\text{melt}) = 2Fe^{3+}AlO_3(\text{perovskite}) + Fe^0(\text{metal}). \quad (1)$$

The magma ocean was gradually oxidized with increasing fO_2. It was estimated [14] that $\Delta \log fO_2$ (IW) increased from −4 to −2, where

$\Delta \log fO_2\,(IW) = \log fO_2\,(IW) - \log fO_2^{(mantle)}$, $fO_2(IW)$ and $fO_2^{(mantle)}$ are the oxygen fugacities of the IW buffer and the mantle, respectively.

According to the concepts of multistage formation of the Earth's core [13], reducing conditions were characteristic of the mantle during its earliest stage over the first 100 Myr of Earth history. The second stage was related to the interaction of the silicate mantle and the core and lasted for the following 150–300 Myr. This stage was accompanied by an increase in fO_2 in the planetary interiors owing to FeO disproportionation in the mantle via the reaction

$$3Fe^{2+}O(mantle) \longrightarrow Fe^0\,(core) + Fe_2^{3+}O_3(mantle). \quad (2)$$

According to [7, 10, 15], the fractionation of Si during mantle–core interaction,

$$SiO_2(silicate) + 2Fe(metal) = Si(metal) + 2FeO(silicate) \quad (3)$$

increases the abundance of FeO and, correspondingly, fO_2 in the mantle. Modeling showed that the incorporation of Si in the core resulted in the gradual oxidation of the mantle, and $\Delta \log fO_2\,(IW)$ increased from −3.2 to −1.4 [15] or from −4.5 to −2.5 [7].

The significant change in redox conditions in the Earth's early mantle owing to the segregation of the metallic phase and evolution of the metallic core allows us to suppose a change in the composition of volatile compounds of C, N, H, and O and their speciation in magmas. Many aspects of this process, which controlled the evolution of the products of magmatic degassing in Earth history, remain obscure.

Experimental studies of the solubility of C–O–H components in melts at fO_2 values corresponding to the stability of the metallic Fe phase [16] suggest that, in addition to oxidized hydrogen species (OH^- and H_2O) characteristic of magmas from the present-day mantle, compounds with C–H-type bonds (e.g., CH_4 and other molecules with this bond) and molecular hydrogen, H_2, probably formed in the primary melts of the reduced mantle.

A significant fO_2 effect on solubility in magmas was observed for another mantle component, nitrogen. Based on limited experimental data on the influence of fO_2 on N solubility in magmatic melts [17–22] and metallurgical slags [23, 24], it can be supposed that the mechanisms of N dissolution in melts derived from the reduced mantle and those formed at moderate fO_2 values are significantly different. At the fO_2 values of the present-day mantle, which are close to the fO_2 of the fayalite–magnetite–quartz (FMQ) buffer equilibrium, nitrogen solubility in basalt melts is rather low owing to its molecular speciation (N_2) in the structure of silicate liquid (physical dissolution) and amounts to parts of ppm [18, 19]. However, nitrogen solubility increases abruptly up to several hundreds of ppm when fO_2 decreases below the fO_2 value of the Fe–FeO (IW) buffer. This effect is due to a change in the mechanism of nitrogen dissolution, which chemically reacts at such fO_2 values with the silicon–oxygen ions of melts with the formation of nitride and other species (chemical dissolution).

Experimental investigations of nitrogen and hydrogen interaction with $FeO–Na_2O–SiO_2–Al_2O_3$ melts at 4 GPa and 1550°C [22] and $Na_2Si_2O_5$ and $Na_2Si_4O_9$ melts at 1.0–2.5 GPa [25] at $fO_2 < fO_2(IW)$ demonstrated that nitrogen is dissolved in silicate liquids as compounds with N–H bonds (NH_3, NH_4^+, etc.) and N_2 molecules.

This study focused on the characteristics of the simultaneous dissolution of hydrogen, nitrogen, and carbon in silicate melt ($FeO–Na_2O–SiO_2–Al_2O_3$) at fO_2 values corresponding to the T–P–fO_2 range of metallic phase stability at pressures lower than in the previous studies [21, 22]. In addition to fO_2, pressure is a factor that can affect the formation of N–C–H species in reduced magmatic melts, but the character of this influence is still poorly understood.

EXPERIMENTAL AND ANALYTICAL METHODS

The finely ground starting mixture for the experiments consisted of 80% albite ($NaAlSi_3O_8$) glass and 20% FeO; 3, 5, and 7 wt % of powdered silicon nitride, Si_3N_4, were added to it as a source of nitrogen in the system. The albite glass was prepared from the SiO_2, Al_2O_3, and Na_2CO_3 reagents preliminarily dehydrated at 1100°C (SiO_2 and Al_2O_3) and ~200°C (Na_2CO_3). The stoichiometric albite mixture of oxides and carbonate was ground for 3 hr in an agate mortar under ethanol. Then, the mixture was decarbonated by heating up to 900°C at a rate of ~10°C/min in an alundum crucible in an argon atmosphere at 1 atm and sintered at 900 and 1 atm for 3–4 hr. After quenching, the decarbonated mixture was reground and melted in a graphite crucible at 1400°C and 1 atm in an argon flow for 3–4 hr. The samples were quenched at a rate of ~100–200°C/s. The homogeneity of the synthetic product was checked by analyzing at least three different glass fragments. The synthetic albite glass was pulverized to a grain size of <20 μm. The desired amounts of FeO and Si_3N_4 dried for 24 hr at 200 and 105°C, respectively, were added to the glass. The albite glass + FeO + Si_3N_4 mixture was ground for 3 hr in an agate mortar under ethanol, dried at 105°C for 6 hr, and kept in a desiccator before being used in experiments. The compositions of the starting mixtures are given in Table 1.

Table 1. Chemical compositions of starting mixtures, wt %

Run	Starting mixture	SiO_2	Al_2O_3	Na_2O	FeO	Si	N	Total
3S*	97%(Ab(80) + FeO(20)) + 3%Si_3N_4	53.34	15.08	9.17	19.40	1.80	1.20	100.00
6S	97%(Ab(80) + FeO(20)) + 3%Si_3N_4	53.34	15.08	9.17	19.40	1.80	1.20	100.00
7S	95%(Ab(80) + FeO(20)) + 5%Si_3N_4	52.24	14.77	8.98	19.00	3.00	2.00	100.00
8S	93%(Ab(80) + FeO(20)) + 7%Si_3N_4	51.14	14.46	8.79	18.60	4.20	2.80	100.00

* Experiment was performed using a Pt capsule without a graphite disk.
Note: Ab is albite, $NaAlSi_3O_8$.

The experiments were performed using a piston–cylinder apparatus [26] at 1.5 GPa and 1400°C in welded platinum capsules. The construction of the high-pressure cell is shown in Fig. 1. The experimental method was described in detail elsewhere [27]. Natural fluorite with low internal friction was used as a pressure-transmitting medium. Temperature was controlled by a Pt–$Pt_{10}Rh$ thermocouple with an accuracy of ±10°C, and the uncertainty of pressure measurement was ±0.1 GPa. Approximately 200 mg of a sample were loaded into a Pt capsule of 5 mm diameter, 15 mm height, and 0.2 mm wall thickness. A 0.2-mm-thick graphite disk was placed beneath the sample. In order to avoid the interaction of the Fe-bearing sample with the walls of the Pt capsule, the sample was isolated by a 0.05-mm-thick W foil [28]. The Pt capsule was packed in powdered boron nitride. The duration of experiments was 2 hr. Quenching was performed by shutting off heating power. In order to prevent decompression-induced capsule rupture, pressure was maintained constant during cooling. The initial cooling rate was ~200°C/s.

The method of buffering hydrogen and oxygen fugacities (fH_2 and fO_2, respectively) was described in detail in [9, 16, 27]. It is based on H_2 diffusion through the walls of the Pt capsule with the attainment of equal chemical potentials of H_2 inside the capsule and in the external solid-media furnace assembly of the apparatus. The values of fH_2 in the solid assembly were imposed by the reaction of traces of H_2O with metallic components of the heating system at fO_2 approaching the iron-wustite buffer equilibrium (Fe–FeO, IW) [16, 28]. Correspondingly, under given T, P, and fO_2 values, fH_2O/fH_2 is fixed in the O–H system outside the capsule. Inside the Pt capsule, fO_2 is controlled by equilibrium between the graphite disk, externally buffered H_2, and the components of Fe-bearing silicate melt. The latter is reduced with the release of O_2 and precipitation of metallic Fe through the reaction

$$2FeO = 2Fe + O_2. \quad (4)$$

Silicon nitride, Si_3N_4, is unstable under the experimental conditions and is completely consumed in the reaction

$$Si_3N_4 \text{ (starting mixture)} + O_2 = 3SiO_2 \text{ (melt)} + 2N_2 \text{ (melt)} \quad (5)$$

with the subsequent reaction of nitrogen with the components of silicate melt, carbon, and hydrogen. Equilibria (4) and (5) control fO_2 in the system during

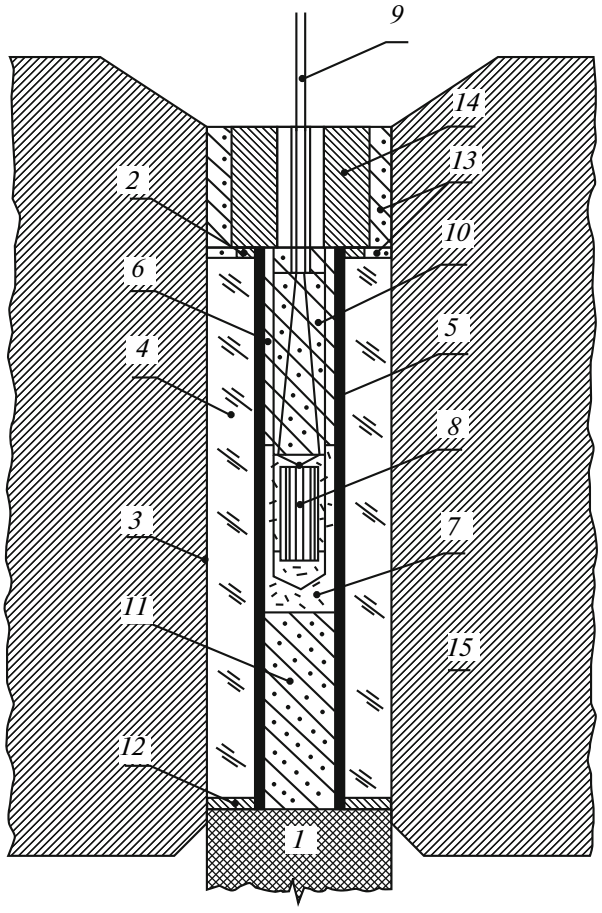

Fig. 1. Scheme of the piston–cylinder high-pressure apparatus: *1*—piston, *2*—upper conducting copper ring, *3*—lead foil, *4*—fluorite sleeve, *5*—graphite heater, *6*—upper pyrophyllite spacer, *7*—boron nitride spacer, *8*—capsule with the sample, *9*—thermocouple, *10*—small pyrophyllite spacer, *11*—lower pyrophillite spacer, *12*—lower conducting copper ring, *13*—insulating pyrophyllite sleeve, *14*—power lead, and *15*—high-pressure vessel.

experiments. Owing to the interaction of Si_3N_4 with silicate melt and O_2 produced by reduction reaction (4), fO_2 within the Pt capsule is much lower than the Fe–FeO (IW) value. The decrease of fO_2 is proportional to the amount of Si_3N_4 in the starting mixture.

The experimental $f\,O_2^{exp}$ values were expressed relative to fO_2 of the Fe–FeO (IW) buffer as

$$\Delta \log fO_2(\mathrm{IW}) = \log fO_2(\mathrm{IW}) - \log fO_2^{exp}, \quad (6)$$

where fO_2(IW) and $f\,O_2^{exp}$ are the oxygen fugacities of the IW buffer and in the experimental sample, respectively. The $f\,O_2^{exp}$ values were obtained from the empirical relation [29]

$$\log f\,O_2^{exp} = 2\log(X_{FeO}/a_{Fe}) - h/T(\mathrm{K}) - \Sigma d X_i), \quad (7)$$

which is based on experimental data on liquid iron–silicate melt equilibria in natural and model magmatic systems. In Eq. (7), h and d are the regression parameters, X_i are the fractions of oxides in silicate melt (mol %), $a_{Fe} = x_{Fe}\,\gamma_{Fe}$ is the activity of Fe in metal alloy, x_{Fe} is the mole fraction of Fe, and γ_{Fe} is the activity coefficient of Fe. In our calculations, γ_{Fe} was assumed to be 1. This assumption is based on the fact that γ_{Fe} is close to one in Fe-rich alloys, and the mole fraction of Fe in the experimental alloys was 0.90–0.98. The fO_2(IW) values were calculated using the experimental data of [30].

The experimental products were analyzed using a Cameca CAMEBAX SX-100 electron microprobe with four vertical spectrometers at the Vernadsky Institute of Geochemistry and Analytical Chemistry, Russian Academy of Sciences. All of the elements were measured simultaneously at an accelerating voltage of 15 kV, a beam current of 30 nA, and an electron beam diameter of 5 μm. Nitrogen was measured using a PC2 pseudocrystal with the interplanar spacing 2d = 97.46 Å. In order to improve the statistical characteristics of analysis, the counting time on the nitrogen peak was increased up to 30 s. BN ceramic was used as a standard for nitrogen analysis. The detection limit for nitrogen was 0.3 wt %.

The $^1H^+/^{30}Si^+$ ratio of glasses was determined using a Cameca IMS 3*f* ion microprobe (Yarslavl Filial of the Physical Technical Institute of the Russian Academy of Sciences). Polished sample mounts were ultrasonically cleaned and coated with Au. The intensities of $^1H^+$ and $^{30}Si^+$ peaks were measured at the bombardment by an O_2^- beam with an intensity of 10–15 nA, a diameter of 10 μm, a mass resolution of 1200, and an energy filtration of 100 ± 20 eV. The $^1H^+/^{30}Si^+$ ratio was estimated using a calibration curve [31], which is characterized by the absence of a matrix effect on the results of measurements at SiO_2 contents between 49 and 71 wt %.

The Raman spectroscopy of N–H–C-bearing glasses was carried out at the Research Center of Fiber Optics, Russian Academy of Sciences. Raman spectra were recorded in 180° backscattering geometry using a triple Jobin Yvon T-64000 spectrometer equipped with a CCD detector cooled with liquid nitrogen. The Raman spectra were excited by an Ar^+ laser (Spectra Physics) radiation with a wavelength of 514.5 nm (5145 Å) focused to a spot of 2 μm diameter on the sample surface through a microscope with a 50× objective. The scattered radiation was collected by the same microscope. The accuracy of the determination of band position was no worse than 1 cm^{-1}.

EXPERIMENTAL RESULTS

Experiments were carried out at 1.5 GPa, 1400°C, and $\Delta \log fO_2$ (IW) of −1.9 (run 3S), −2.1 (run 6S), −2.4 (run 7S), and −3.7 (run 8S). The experimental products are transparent glasses with globules of metallic Fe smaller than 50 μm (Fig. 2). The color of the glass depends on the experimental conditions and varies from golden yellow (run 3S) to greenish (runs 7S and 8S). The spherical shape of the Fe metal suggests its liquid state during the experiments. Microscopic examination did not reveal gas inclusions in the glasses, which indicates that the melt was not saturated with respect to N–C–H volatile compounds.

A characteristic feature of the chemical compositions of glasses is a decrease in FeO content from ~19 wt %, which is equal to that of the starting mixture (Table 1), to 1.6 wt % at the lowest $\Delta \log fO_2$ (IW) values (Table 2). This is indicative of FeO reduction in the melt with the formation of liquid Fe in accordance with reaction (4).

Reactions (4) and (5) suggest that the SiO_2 content of melt is controlled by two processes: the removal of FeO from the melt owing to the formation of liquid Fe and oxidation of Si_3N_4 in the starting mixture resulting in the addition of a certain amount of SiO_2 to the melt. This is illustrated by the SiO_2–FeO diagram (Fig. 3) for the experimental melts compared with SiO_2 contents calculated taking into account only FeO reduction. The observed SiO_2–FeO covariations show higher SiO_2 contents in the experimental glasses, which could be expected considering the contribution of reaction (5) to the formation of the composition of silicate liquid. In addition to optical examination, the chemical composition of glasses indicates that Si_3N_4, which was added to the experimental starting materials, is unstable under the experimental conditions and was completely consumed by reaction (5).

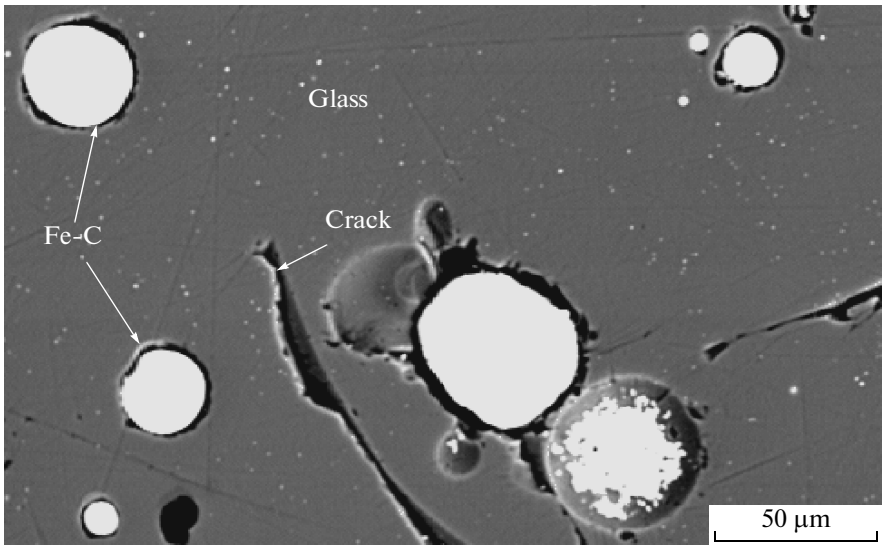

Fig. 2. Back-scattered electron image of quenched glass with droplets of metallic iron in the products of run 8S at $P = 1.5$ GPa, $T = 1400°C$, and $\Delta\log fO_2$ (IW) = −3.7.

The distribution of FeO, Na_2O, Al_2O_3, SiO_2, N, and C in the glasses is relatively homogeneous, which suggests the attainment of chemical equilibrium during the experiments (Fig. 4).

The glasses contain 0.5–1.5 wt % N and 0.4–0.8 wt % C (Table 2, Fig. 5). The highest N and C contents were observed in the glasses from the lowest fO_2 experiments at $\Delta\log fO_2$ (IW) = −3.7. The content of H in the glasses is 0.3–0.6 wt % and decreases with decreasing fO_2 (Fig. 5).

The globules of metallic phase contain 0.7–1.8 wt % N and 0.5–0.8 wt % C (Table 2).

The Raman spectra of glasses within 2000–4150 cm^{-1} display several peaks, which can be assigned to complexes or molecules with O–H, N–H, N–N, and H–H bonds (Fig. 6).

O–H bonds. The Raman spectra of glasses display a broad asymmetric band in the high-frequency region centered at 3561 cm^{-1}. The shape of the band is similar to that observed in hydrogen-bearing glasses in the Na_2O–Al_2O_3–SiO_2 and other systems [32]. It is assigned to O–H vibrations in OH^- groups and H_2O molecules in the structure of silicate melts.

N–H bonds. The spectral investigations of nitrogen speciation in the glasses of the Na_2O–SiO_2 [25] and

Table 2. Chemical compositions of glasses and the metallic phase after experiments at 1.5 GPa and 1400×C, wt %

Glass

Run	$\Delta\log fO_2$ (IW)	SiO_2	Al_2O_3	Na_2O	FeO	N	C	Total
3S	−1.9	63.48(21)	15.26(12)	8.39(10)	10.73(10)	0.47(13)	0.64(21)	98.97
6S	−2.1	67.82(26)	12.8(10)	7.36(15)	9.78(14)	0.62(19)	0.65(19)	99.03
7S	−2.4	70.03(41)	13.74(17)	8.11(24)	6.93(39)	0.60(19)	0.40(20)	99.81
8S	−3.7	74.71(20)	13.42(20)	7.55(13)	1.58(8)	1.47(24)	0.84(15)	99.57

Metallic globules

Run	$\Delta\log fO_2$ (IW)	Fe	Si	Al	N	C	W	Total
7S	−2.4	96.92(19)	0.04(1)	0.02(1)	1.75(17)	0.84(16)	0.16(13)	99.68
8S	−3.7	97.90(75)	0.05(1)	0.02(1)	0.71(21)	0.45(18)	0.12(9)	99.59

The analyses are averages of 10 determinations of oxides and elements for glasses and 5 determinations for the metallic phase, and standard deviation is shown in parentheses. The compositions of metallic phase were not determined in experiments 3S and 6S because of the small sizes of the globules (<10 mm).

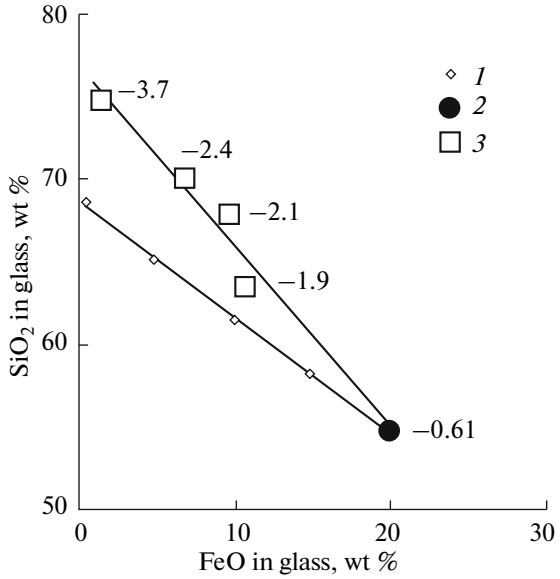

Fig. 3. SiO_2 content in glasses as a function of FeO content: (*1*) calculated SiO_2 variations due to FeO reduction only; (*2*) contents of SiO_2 and FeO in the starting mixture $NaAlSi_3O_8$ (80 wt %) + FeO (20 wt %) at $\Delta\log fO_2$ (IW) = –0.61 corresponds to melt equilibrium with the Fe metallic phase at 1.5 GPa and 1400°C; and (*3*) contents of SiO_2 and FeO in glasses controlled by fO_2 values during the experiments: run 3S at $\Delta\log fO_2$ (IW) = –1.9, run 6S at $\Delta\log fO_2$ (IW) = –2.1, run 7S at $\Delta\log fO_2$ (IW) = –2.4, and run 8S at $\Delta\log fO_2$ (IW) = –3.7.

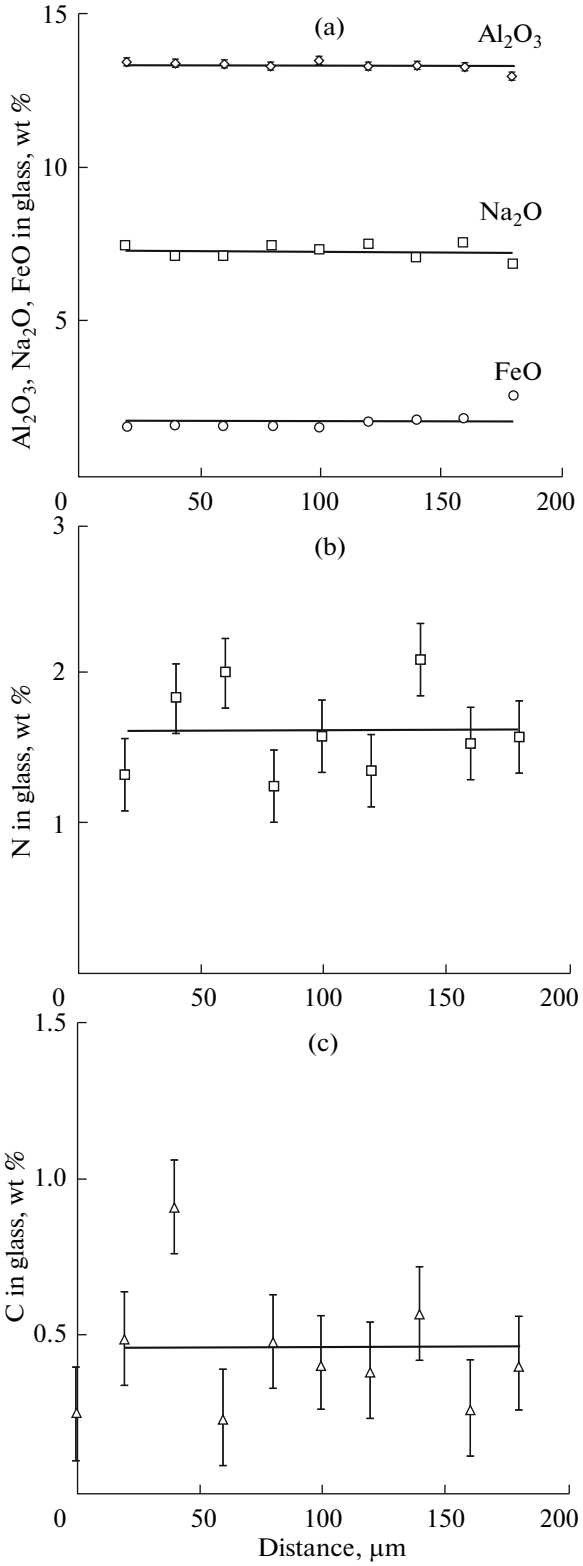

Fig. 4. Contents of (a) FeO, Na_2O, Al_2O_3, (b) N, and (c) C in glass along a profile from the rim of an iron droplets from run 8S ($\Delta\log fO_2$ (IW) = –3.7).

$FeO–Na_2O–Al_2O_3–SiO_2$ systems [22] obtained at 1–2 GPa, 1300–1500°C and 4 GPa, 1550°C, respectively, showed that a narrow intense absorption band at 3293 cm^{-1} and bands at 3377 and 3188 cm^{-1} correspond to complexes or molecules with N–H bonds, including NH_3, NH_2^- (≡Si–NH_2), and NH_2^+ (O–NH_2). According to [25], the peak at 2912 cm^{-1} corresponds to the vibrations of N–H bonds in NH_2^+ (O–NH_2).

N–N bonds. The narrow sharp peak at 2331 cm^{-1} is assigned to molecular nitrogen dissolved in glass. At normal temperature and pressure, the vibration of N–N bonds in N_2 molecules corresponds to 2331 cm^{-1}. However, this band of N_2 molecules in glass is wider than that of N_2 in air. A similar band of N_2 in glass was observed [20, 22] during the investigation of the solubility of nitrogen and its hydrogen-bearing compounds in silicate melts at high temperatures.

H–H bonds. A weak band at 4133 cm^{-1} is related to molecular H_2 dissolved in glass [33, 34].

Thus, the spectral investigation showed that N–H species (NH_3, NH_2^-, and NH_2^+) and molecular N_2 are formed in silicate glasses of the $FeO–Na_2O–Al_2O_3–$

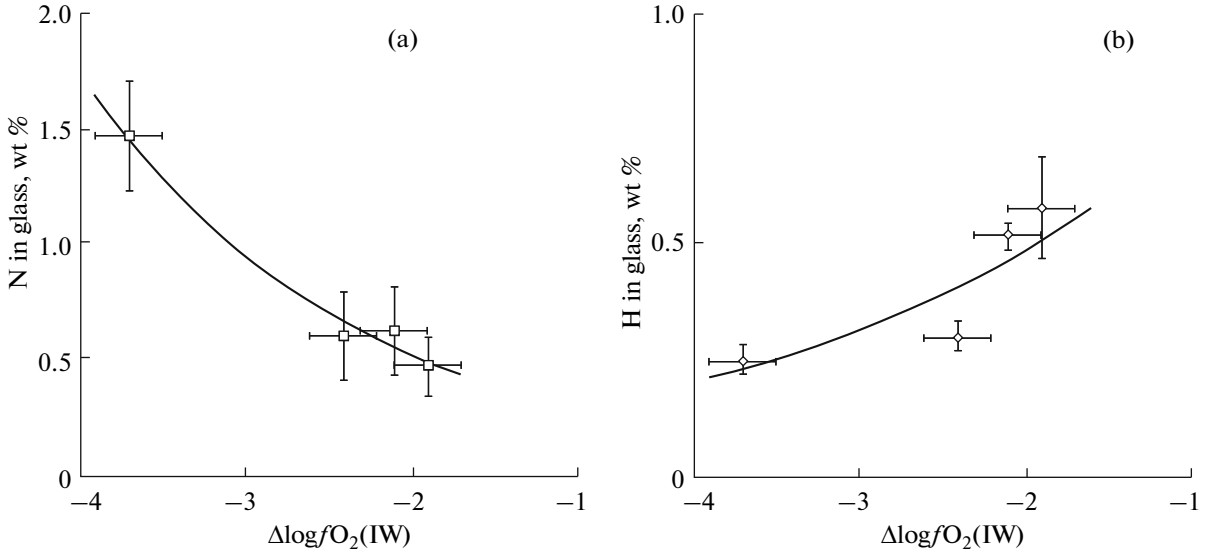

Fig. 5. Contents of (a) nitrogen and (b) hydrogen in Fe-bearing silicate melt as a function of oxygen fugacity.

SiO_2 system in equilibrium with metallic Fe. Hydrogen occurs in melts as OH^- groups, H_2O molecules, and molecular H_2.

The speciation of nitrogen and hydrogen dissolved in $FeO–Na_2O–SiO_2–Al_2O_3$ melts at a pressure of 1.5 GPa and a temperature of 1400°C is identical to that observed previously in $FeO–Na_2O–SiO_2–Al_2O_3$ melts at 4 GPa, 1550°C, and similar fO_2 values [22]. It can be concluded that a pressure decrease from 4 to 1.5 GPa did not affect the speciation of N and H in silicate melts in equilibrium with metallic Fe.

PETROLOGICAL APPLICATIONS: CHARACTER OF MAGMATIC DEGASSING OF THE EARTH'S EARLY MANTLE

The regime of fO_2 during magma ocean formation is of profound importance for the estimation of the composition of gases extracted from a reduced planetary material to the surface during high-temperature volcanic activity. Experimental investigations at 1.5 GPa and 1400°C showed that melting in the stability field of metallic Fe in the presence of hydrogen produces silicate liquids containing compounds with N–H bonds in addition to molecular N_2 and H_2. A remarkable feature of redox reactions in melts is that, despite low fO_2 values, species with O–H bonds (OH^- and H_2O) are formed in them. Hence, it can be suggested that the degassing product of the early reduced mantle in equilibrium with a metallic phase contained primary magmatic water, in addition to N_2, nitrogen compounds, and hydrogen.

The formation of N–H bonds in molten silicates significantly increases nitrogen solubility, which can be as high as 0.5–1.5 wt % at $\Delta \log fO_2$ (IW) between −1.9 and −3.7. Thus, the melting products of the early Earth were probably richer in nitrogen compared with the magmas of later geologic epochs with fO_2 values higher than fO_2(IW). In the latter case, the solubility of nitrogen in the form of N_2 molecules is $n \times 10^{-4}$ wt % [18, 19].

The change in the mechanism of nitrogen dissolution at fO_2 values significantly lower than fO_2 characteristic of the present-day mantle is of fundamental importance for the understanding of the geochemical history of nitrogen. In addition to isotopic composition, the behavior of nitrogen in deep mantle reservoirs is constrained in modern geochemistry by the similarity of its behavior to that of noble gases. This similarity is supported by the common physical nature of the dissolution of these volatiles in silicate liquids at certain P–T–fO_2 conditions.

The solubility of nitrogen is most comparable with that of argon, which was established by several authors for basaltic melts at ambient pressure and temperatures between 1300 and 1650°C [35–39]. The similarity between the solubilities is due to their similar atomic sizes. They fill space within the structure of silicate melt in identical fashion. The similarity of the physical solubilities of N and Ar suggests that the N/Ar ratio is not significantly affected by magma differentiation and can be used for the estimation of nitrogen behavior during mantle degassing and atmosphere formation. However, some investigations [18–20, 22] and the present experiments showed that the similarity in the solubility of nitrogen and noble gases is restricted to the redox conditions of magma generation in the mantle. The similarity of the solubilities of

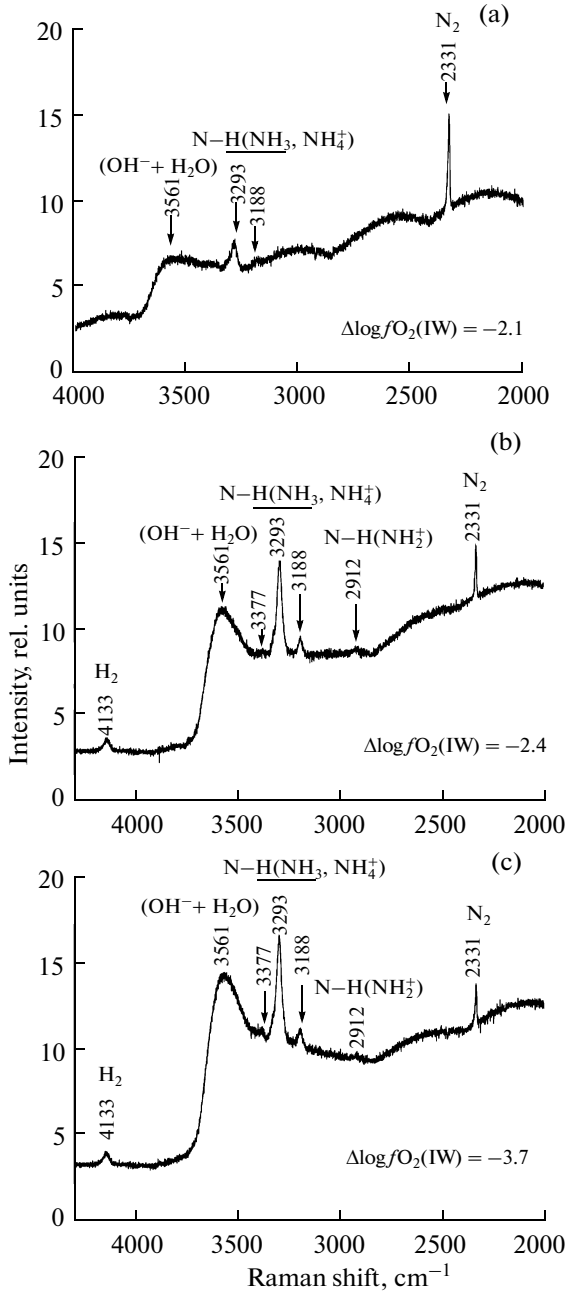

Fig. 6. Raman spectra of N–H-bearing glasses synthesized at $P = 1.5$ GPa and $T = 1400$°C: (a) run 6S, $\Delta\log fO_2$ (IW) = –2,1; (b) run 7S, $\Delta\log fO_2$ (IW) = –2.4; and (c) run 8S, $\Delta\log fO_2$ (IW) = –3.7.

N and noble gases is violated at fO_2 values below fO_2(IW), when the chemical interaction of nitrogen with silicate melts causes the formation of N–H complexes. Therefore, the N/Ar ratio cannot be used for the analysis of the geochemical history of nitrogen related to its dissolution and degassing during the melting of the early reduced mantle.

Experimental investigations [22] revealed significant effects of pressure and fO_2 on the partition coefficient of nitrogen between FeO–Na_2O–SiO_2–Al_2O_3 melt and the equilibrium metallic phase ($D_N = N^{metal}/N^{silicate}$). It was found that D_N is 0.82 at 4 GPa, 1550°C, and $\Delta\log fO_2$ (IW) = –3.3, whereas D_N is much higher and approaches 10^4 at normal N_2 pressure, 1600°C, and $fO_2 = fO_2$(IW) [18]. A similar dependence of nitrogen partitioning between FeO–Na_2O–SiO_2–Al_2O_3 melt and the equilibrium metallic phase was observed in our experiments at 1.5 GPa and 1400°C: D_N is 2.9 at $\Delta\log fO_2$ (IW) = –2.4 and 0.5 at $\Delta\log fO_2$ (IW) = –3.7.

The significant decrease of D_N compared with ambient pressure is a direct consequence of an increase in nitrogen solubility in silicate melt and liquid Fe metal at high pressures, fO_2 below fO_2(IW), and in the presence of hydrogen in the system. The experimental results indicate that the ability of silicate melt to extract nitrogen from the early mantle appears to be similar under such conditions to that of the molten metallic alloy. This enhances the role of magmas in nitrogen transport from the interiors of the early Earth to its surface during the short period of the geochemical history of the Earth when the planetary core was formed at low fO_2 values in the mantle.

An increase in fO_2 owing to the interaction of the core with mantle components at the last stages of core formation [13] or during the generation and evolution of the magma ocean [40] resulted in a decrease in nitrogen solubility in melting products and, correspondingly, a change in the conditions of its magmatic transport toward the Earth's surface.

CONCLUSIONS

The investigation of the system silicate melt (FeO–Na_2O–SiO_2–Al_2O_3) + liquid metallic Fe + C (graphite) + volatile components (N–C–H) at 1.5 GPa, 1400°C, and fO_2 from 1.9 to 3.7 logarithmic units lower than the fO_2(IW) values revealed the formation of hydrogen-bearing nitrogen species (NH_3, NH_2^-, and NH_2^+) and molecular nitrogen (N_2) in silicate melts. Hydrogen occurs in the melt as hydroxyl groups (OH^-), molecular water (H_2O), and molecular hydrogen (H_2).

Oxygen fugacity strongly influences the solubility and speciation of nitrogen in the melts: as fO_2 decreases, the solubility of nitrogen increases, the fraction of molecular nitrogen decreases, and the fraction of species with N–H bonds increases.

The formation of N–H bonds in molten silicates results in a significant increase in nitrogen solubility, which may be as high as 0.5–1.5 wt % at $\Delta \log fO_2$ (IW) values between –1.9 and –3.7. It can be suggested, therefore, that the melting products of the early Earth were richer in nitrogen compared with the magmas of later geologic epochs formed at fO_2 higher than fO_2(IW).

Even at low fO_2 values, species with O–H bonds (OH^-, H_2O) are formed in melts; i.e., the products of the degassing of the early reduced mantle in equilibrium with a metallic phase could contain primary magmatic water coexisting with N–H species, molecular N_2, and H_2.

It was shown that pressure and fO_2 have a profound influence on the partition coefficient of nitrogen between silicate melt and the equilibrium metallic phase ($D_N = N^{metal}/N^{silicate}$). At 1.5 GPa and 1400°C, D_N is 2.9 at $\Delta \log fO_2$ (IW) = –2.4 and 0.5 at $\Delta \log fO_2$ (IW) = –3.7.

ACKNOWLEDGMENTS

This study was financially supported by the Russian Foundation for Basic Research, project no. 08-05-00377, Program no. 24 of the Presidium of the Russian Academy of Sciences, and Program no. 8 of the Department of Earth Sciences of the Russian Academy of Sciences.

REFERENCES

1. D. Stevenson, "Models of the Earth's Core," Science **214**, 611–619 (1981).
2. S. Sasaki and K. Nakazawa, "Metal–Silicate Fractionation in the Growing Earth: Energy Source for the Terrestrial Magma Ocean," J. Geophys. Res. **91**, B9231–B9238 (1986).
3. H. Melosh, "Giant Impacts and the Thermal State of the Early Earth," in *Origin of the Earth,* Ed. by H. E. Newsom and J. H. Jones (Oxford Univ., New York, 1990), pp. 69–83.
4. J. Li and C. B. Agee, "Geochemistry of Mantle–Core Differentiation at High Pressure," Nature **381**, 686–689 (1996).
5. K. Righter and M. J. Drake, "Metal/Silicate Equilibrium in the Early Earth—New Constraints from the Volatile Moderately Siderophile Elements Ga, Cu, P, and Sn," Geochim. Cosmochim. Acta **64**, 3581–3597 (2000).
6. B. J. Wood, M. J. Walter, and J. Wade, "Accretion of the Earth and Segregation of Its Core," Nature **441**, 825–833 (2006).
7. D. J. Frost, U. Mann, Y. Asahara, and D. C. Rubie, "The Redox State of the Mantle during and Just after Core Formation," Philos. Trans. R. Soc. **A366**, 4315–4337 (2008).
8. J. W. Delano, "Redox History of the Earth's Interior since ~3900 Ma: Implications for Prebiotic Molecules," Origin of Life and Evolution of the Biosphere **31**, 311–341 (2001).
9. A. A. Kadik, Yu. A. Litvin, V. V. Koltashev, et al., "Solubility of Hydrogen and Carbon in Reduced Magmas of the Early Earth's Mantle," Geokhimiya, No. 1, 38–53 (2006) [Geochem. Int. **44**, 33–47 (2006)].
10. M. Javoy, "The Integral Enstatite Chondrite Model of the Earth," Geophys. Res. Lett. **22**, 2219–2222 (1995).
11. D. J. Frost, C. Liebske, F. Langenhorst, et al., "Experimental Evidence for the Existence of Iron-Rich Metal in the Earth's Lower Mantle," Nature, **428** (6981), 409–412 (2004).
12. D. C. Rubie, C. K. Gessmann, and D. J. Frost, "Partitioning of Oxygen during Core Formation on the Earth and Mars," Nature **429**, 58–62 (2004).
13. E. M. Galimov, "Redox Evolution of the Earth Caused by a Multistage Formation of Its Core," Earth Planet. Sci. Lett. **233**, 263–276 (2005).
14. J. Wade and B. J. Wood, "Core Formation and the Oxidation State of the Earth," Earth Planet. Sci. Lett. **236**, 78–95 (2005).
15. M. Javoy, E. Kaminski, F. Guyot, et al., "The Chemical Composition of the Earth: Enstatite Chondrite Models," Earth Planet. Sci. Lett. **293**, 259–268 (2010).
16. A. A. Kadik, F. Pineau, Yu. A. Litvin, et al., "Formation of Carbon and Hydrogen Species in Magmas at Low Oxygen Fugacity," J. Petrol. **45** (7), 1297–1310 (2004).
17. R. A. Fogel, "Nitrogen Solubility in Aubrite and E Chondrite Melts," Lunar Planet. Sci. Conf. **25**, 383–384 (1994).
18. A. Miyazaki, H. Hiyagon, N. Sugiura, et al., "Solubilities of Nitrogen and Noble Gases in Silicate Melts under Various Oxygen Fugacities: Implications for the Origin and Degassing History of Nitrogen and Noble Gases in the Earth," Geochim. Cosmochim. Acta **68** (2), 387–401 (2004).
19. G. Libourel, B. Marty, and F. Humbert, "Nitrogen Solubility in Basaltic Melt. Part I. Effect of Oxygen Fugacity," Geochim. Cosmochim. Acta **67** (21), 4123–4135 (2003).
20. M. Roskosz, B. O. Mysen, and G. D. Cody, "Dual Speciation of Nitrogen in Silicate Melts at High Pressure and Temperature: An Experimental Study," Geochim. Cosmochim. Acta **70**, 2902–2918 (2006).
21. A. A. Kadik and Yu. A. Litvin, "Magmatic Transport of Carbon, Hydrogen, and Nitrogen Constituents from Reduced Planetary Interiors," Lunar Planet. Sci. **38**, LPI Contrib., No. 1338, 1020 (2007).
22. A. A. Kadik, Yu. A. Litvin, V. V. Koltashev, et al., "Role of Hydrogen and Oxygen Fugacity in Incorporation of Nitrogen in Reduced Magmas of the Early Earth's Mantle," J. Petrol. (in press).
23. H. O. Mulfinger, "Physical and Chemical Solubility of Nitrogen in Glass Melts," J. Am. Ceram. Soc. **49**, 462–467 (1966).
24. C. Schrimpf and G. H. Frischat, "Property–Composition Relations of N_2-Containing Na_2O–CaO–SiO_2 Glasses," J. Non-Cryst. Solids **56**, 153–160 (1983).
25. B. O. Mysen, S. Yamashita, and N. Chertkova, "Solubility and Solution Mechanisms of NOH Volatiles in

Silicate Melts at High Pressure and Temperature—Amine Groups and Hydrogen Fugacity," Am. Mineral. **93**, 1760–1770 (2008).

26. A. B. Slutskii, "Apparatus for Geochemical Studies under Super-High Pressures and Temperatures," in *Experimental Studies of Endogenous Processes* (Izd-vo Akademii nauk SSSR, Moscow, 1962), pp. 212–215 [in Russian].
27. A. A. Kadik, N. A. Kurovskaya, Yu. A. Ignat'ev, et al., "Influence of Oxygen Fugacity on the Solubility of Carbon and Hydrogen in $FeO–Na_2O–SiO_2–Al_2O_3$ Melts in Equilibrium with Liquid Iron at 1.5 GPa and 1400°C," Geokhimiya, No. 10, 1011–1018 (2010) [Geochem. Int. **48**, 953–960 (2010)].
28. Yu. A. Litvin, "Technique of High-Pressure Studies of Phase Equilibria with Participation of Fe-Bearing Magmatic Melts," Geokhimiya, No. 8, 1234–1242 (1981).
29. A. A. Ariskin, A. A. Borisov, and G. S. Barmina, "Modeling of Iron–Silicate Melt Equilibrium in Basaltic Systems," Geokhimiya, No. 9, 1231–1240 (1992).
30. H. S. C. O'Neill and M. I. Pownceby, "Thermodynamic Data from Redox Reactions at High Temperatures: I. An Experimental and Theoretical Assessment of the Electrochemical Method Using Stabilized Zirconia Electrolytes, with Revised Values for the Fe–"FeO", Co–CoO, Ni–NiO and Cu–Cu_2O Oxygen Buffers, and New Data for the W—WO_2 Buffer," Contrib. Mineral. Petrol. **114**, 296–314 (1993).
31. A. V. Sobolev and M. Chaussidon, "H_2O Concentrations in Primary Melts from Suprasubduction Zones and Mid-Ocean Ridges: Implications for H_2O Storage and Recycling in the Mantle," Earth Planet. Sci. Lett. **137**, 45–55 (1996).
32. B. O. Mysen and D. Virgo, "Volatiles in Silicate Melts at High Pressure and Temperature. 2: Water in Melts along the Join $NaAlO_2–SiO_2$ and a Comparison of Solubility Mechanism of Water and Fluorine," Chem. Geol. **57**, 333–358 (1986).
33. R. W. Luth, B. O. Mysen, and D. Virgo, "Raman Spectroscopic Study of the Solubility Behavior of H_2 in the System $Na_2O–Al_2O_3–SiO_2–H_2$," Am. Mineral. **72**, 481–486 (1987).
34. E. M. Dianov, V. V. Koltashev, S. N. Klyamkin, et al., "Hydrogen Diffusion and Ortho–Para Conversion in Absorption and Raman Spectra of Germanosilicate Optical Fibers Hydrogen-Loaded at 150–170 MPa," J. Non-Cryst. Solids, **351** (49–51), 3677–3684 (2005).
35. H. Hiyagon and M. Ozima, "Partition of Noble Gases between Olivine and Basalt Melt," Geochim. Cosmochim. Acta **50**, 2045–2057 (1986).
36. A. Jambon, H. Weber, and O. Braun, "Solubility of He, Ne, Ar, Kr and Xe in a Basalt Melt in the Range 1250–1600°C: Geochemical Implications," Geochim. Cosmochim. Acta **50**, 401–408 (1986).
37. G. Lux, "The Behaviour of Noble Gases in Silicate Liquids: Solution, Diffusion, Bubbles and Surface Effects with Application to Natural Samples," Geochim. Cosmochim. Acta **51**, 1549–1560 (1987).
38. M. R. Carroll and D. S. Draper, "Noble Gases as Trace Elements in Magmatic Processes," Chem. Geol. **117**, 37–56 (1994).
39. A. Miyazaki, *Studies on Solubilities of Nitrogen and Noble Gases in Silicate Melts* (Univ. Tokyo, Tokyo, 1996).
40. B. J. Wood, J. Wade, and M. R. Kilburn, "Core Formation and the Oxidation State of the Earth: Additional Constraints from Nb, V and Cr Partitioning," Geochim. Cosmochim. Acta **72**, 1415–1426 (2008).